



BUDAPEST UNIVERSITY OF TECHNOLOGY AND ECONOMICS

**INVESTIGATION OF MICROSTRUCTURE,
ORIENTATION, AND LAYER DEVELOPMENT
DURING COLOR ETCHING**

THESIS BOOKLET

JÓZSEF BÁLINT RENKÓ

MSC IN MECHANICAL ENGINEERING

Supervisors:

PÉTER JÁNOS SZABÓ
professor

ATTILA BONYÁR
associate professor

Faculty of Mechanical Engineering
Department of Materials Science and Engineering
Géza Pattantyús-Ábrahám Doctoral School of Mechanical Engineering

BUDAPEST, 2023

1. INTRODUCTION

Etching is a widely used tool in metallography as it offers a quick and easy solution for developing the microstructure of different samples (Vander Voort, 1986). Although various techniques exist for different purposes, their overall goal is the same: to produce a structure with sufficient contrast over the surface, where the different microstructural elements can be distinguished (Vander Voort, 1984). During etching, the previously polished surface reacts with the applied chemical or beam, revealing certain parts of the microstructure. Depending on the nature of the etchant, grains, grain boundaries, precipitations, or different phases become visually separable, allowing further surface analysis on it (Vander Voort, 1985).

The two most widely used wet etching methods are chemical etchants and color etchants. Chemical etchants are the more frequently used developing tools, as most of the reagents belong to this group. These etchants typically have an acidic pH, resulting in a more aggressive reaction between the etchant and substrate. They dissolve certain parts of the sample's surface into the etching solution. The visualization of the microstructure is based on the difference in their etching rate, as they result in a detectable change in topography (Figure 1.a). Depending on the material-etchant combination, the process usually takes from seconds up to a few minutes (Vander Voort & Manilova, 2023), (Panagopoulos et al., 2009), (Monteiro et al., 2010), (Fleißner-Rieger et al., 2021). Although for most cases, this information is more than enough, these etched surfaces contain no additional information other than revealing microstructure for metallographic examination.

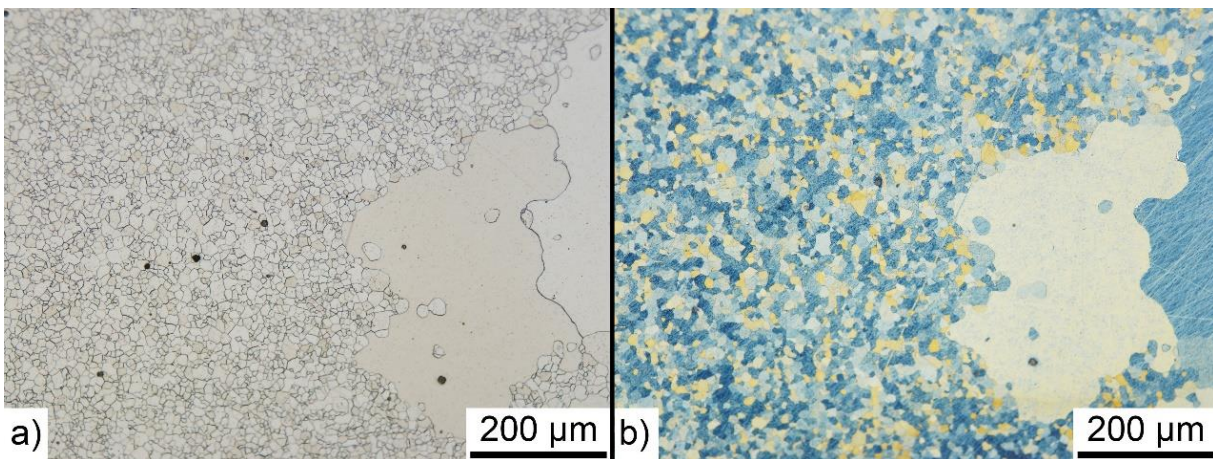


Figure 1. Low-carbon steel surface etched with 2% Nital (a) chemical etchant and Beraha-I (b) color etchant

Contrary to chemical etching, color etchants not only dissolve the base alloy but also develop a film from the mixture of compounds on its surface (Figure 1.b). Hence, the reaction typically occurs over individual grains instead of grain boundaries. As the layer grows, it interferes with the incoming light, resulting in constantly changing colors (Rawdon & Lorentz, 1920). Since the etching rate of grains with different orientations is slightly different as they can resist corrosion to different degrees, stopping the

film development at any moment will result in different precipitation thicknesses over the individual grains, and thus, in orientation-dependent colors (Bonyár & Szabó, 2012). Consequently, color etchants contain additional information about the crystallographic orientation of the grains.

2. PROBLEMS AND AIMS

If the crystallographic orientation distribution of the grains within the polycrystalline aggregate is largely dominated by a single orientation, the material becomes textured (Hölscher et al., 1991). Texture plays an important role in manufacturing because various properties of the crystals, such as crystal plasticity, fracture toughness, electrical conductivity, diffusion, superconductivity, mechanical twinning, corrosion resistance, etc., are very strongly orientation-dependent (Newesely & Rabe, 1985), (Hamelin, 1984), (Tran et al., 2019), (Panda et al., 2014), (Yardley et al., 2014). Consequently, from the aspect of quality control, measuring the crystallographic orientation is essential to describe material properties.

Although the connection between etching rate and orientation was already well known, color etching as a possible tool was utilized much later than chemical etchants because the layer development mechanisms were mostly unknown (Kardos et al., 2007). The possible connection between grains and orientations was typically stuck at the level that “grains with the same color belong to the same orientation” without connecting colors to certain directions (Mandal et al., 2022), (Medina-Mendoza et al., 2022). Additionally, since this research field is relatively new, the layer development mechanisms are not fully understood in depth to draw the proper conclusions (Kardos & Gácsi, 2013), (Britz et al., 2016).

To properly utilize color etching as an orientation determination technique, first, the basic developing mechanisms must be explored. This requires both a measuring and an evaluating method that consider the possible influencing factors while allowing to monitor and understand these mechanisms. Only then do the detected but not yet exploited processes become comprehensible to use color etching for orientation analysis.

In this work, I aim to reveal and explain the necessary but previously unexplored mechanisms of color etching. For this purpose, I will develop both the required measuring tools and calculation methods suitable to combine them with various already existing microstructural testing equipment. After a deeper understanding of the fundamental principles of color etching, I will propose a new method, which leads to determining crystallographic orientation with color etching under an optical microscope without the need for electron backscatter diffractometry (EBSD).

3. ETCHANT AND MATERIALS

Color etchants have various possible applications based on the material to be examined. As my primary focus is the understanding and utilizing of underlying mechanisms of layer development, it is preferable to choose an etchant that could react with different materials but has a relatively slow reaction speed. If the etchant can attack multiple phases and materials, it will be applicable much more widely. A slower etching rate, on the other hand, increases the available time for examinations, which may help better separate parts of the process.

Based on these considerations, Beraha-I was chosen as the etchant (Vander Voort, 2004). This salt solution has no acidic component and has a significantly slower reaction speed than any acidic color etchants. Moreover, it can react with low and moderate corrosion-resistant materials, like low-carbon steel, cast iron, or copper, all of which were examined based on the needs of the given experiment (Jovičević-Klug et al., 2021).

First, to understand the basic etching mechanisms, cast iron was used due to its higher corrosion resistance and heterogeneous surface. Higher corrosion resistance allowed to slow down the etching process to a level where the surface changes could be easily monitored, while spheroidal graphites across the surface could be used to identify the same area multiple times. Later, when a homogeneous surface was required with large grains, DC01 low-carbon steel was used. It contained no secondary phases that could alter results, which was especially useful for the investigation with spectroscopic ellipsometer and with X-ray photoelectron spectroscope, where the spot size was 0.3 mm and 5 mm, respectively. Finally, industrial-grade pure copper (Cu99.9) was also investigated to see how the etching changes if the substrate has a face-centered cubic lattice instead of the base-centered cubic lattice that ferrite had.

4. RESULTS AND DISCUSSION

4.1. Development of novel experimental methods (P2, P5)

In order to gain a more detailed understanding of the processes, in-situ observation is necessary, for which the necessary equipment must be developed. First, compatibility is an important factor, as the equipment must ensure the examination of the sample's surface with the given observation method while the etchant is flowing over its surface. Thus, the equipment must contain a relatively small, closed cavity where the etchant will flow. By minimizing the size of the system, the experiments require less reagent, resulting in smaller diffusion distances, better-controlled flow properties, and faster reactions. Those parts of the equipment that are getting into contact with the etchant must be made from a chemically inert material to avoid any cross-reaction. Reproducibility of the experiment is also crucial, thus, influencing factors, like etchant flow, sample positioning, or flow type (laminar, turbulent) must be controllable. The samples' geometry may also differ, but by embedding samples into vinyl, a general

shape can be created that is suitable for examination regardless of the original form. Manufacturability, replacement of the sample, and cleaning of the system should also be taken into account.

Based on these considerations, two microfluidic cells were developed, one for optical microscopy (OM) and one for spectroscopic ellipsometry (SE). Both cells contain a polydimethylsiloxane (PDMS) body, sealed with glass plates or with the sample from different directions. PDMS is not only chemically inert, but it is transparent and flexible enough to resist any occurring mechanical load (Bonyár et al., 2010). The first microfluidic cell developed for OM is presented in Figure 2.

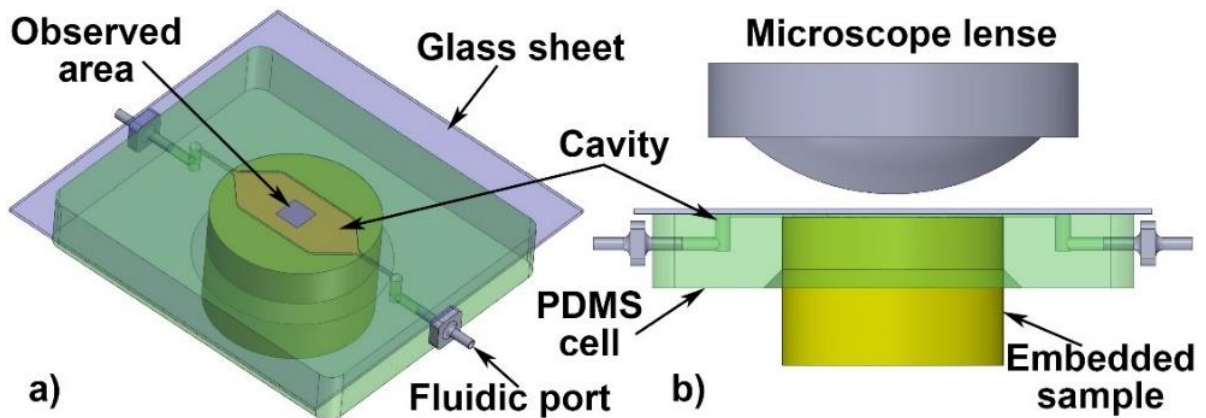


Figure 2. Schematic figure of the microfluidic cell (a) and its position under the optical microscope (b)

For typical SE measurement, the media boundaries should be placed perpendicular to the light path with a diameter of 3 mm, as this is the spot size prior to focusing it. Otherwise, a significant intensity loss occurs, while additional reflections could even alter the results. Considering that the angle of incidence of the incoming light is approx. 55° and the inner cavity must be completely sealed, a second microfluidic cell must be designed so that every occurring boundary in the light path is perpendicular to it. The redesigned microfluidic cell for SE is presented in Figure 3.

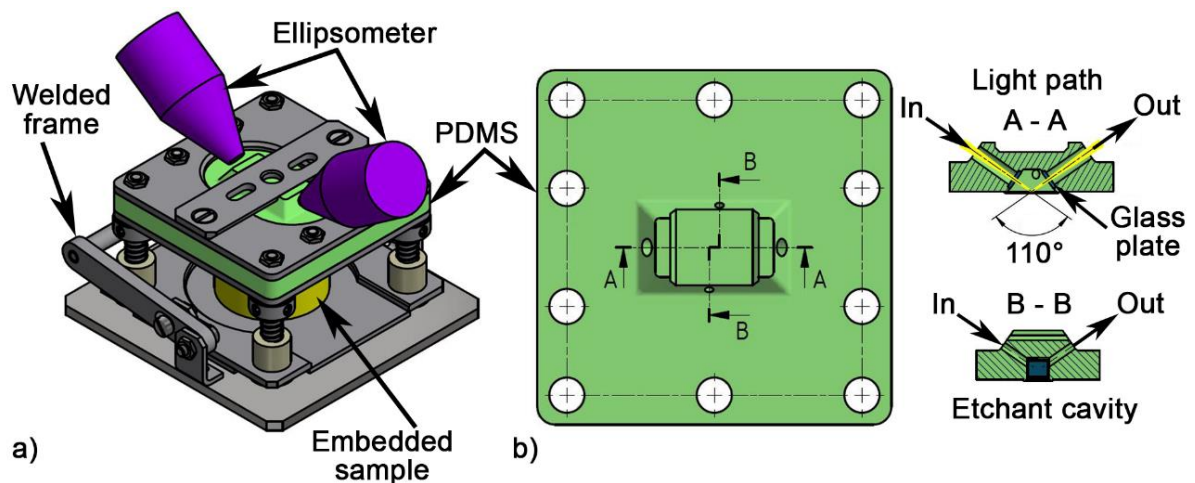


Figure 3. Schematic figure of the microfluidic cell (a) and the inner structure of the PDMS cell (b)

4.2. Analysis of the connection between the crystallographic orientation and the color of the developed layer on etched surfaces (P1)

In the first experiment, spheroidal graphite cast iron was etched with Beraha-I to formulate the initial kinetic model of color etching and demonstrate that the determination of crystallographic orientation is possible with this method. In this kinetic model, the most important factors during color etching that affect the resulting color are the wavelength-dependent refractive index and the layer thickness. Assuming that the precipitation is homogeneous and the refractive index is constant over the individual grains regardless of their orientation, the only difference that results in different colors is the layer thickness. Hence, by assigning the layer thicknesses to etching times, the etching rate can be determined.

By using the first microfluidic cell, the intensity of different wavelengths over the individual grains can be measured, and the RGB intensity change can be visualized. The intensity curves show a sinusoidal character with decreasing amplitude.

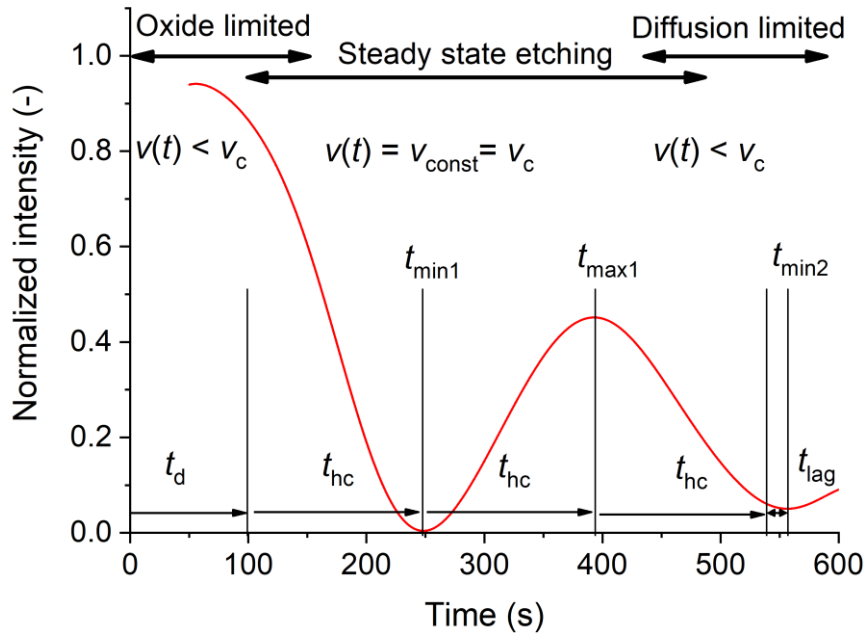


Figure 4. The functional kinetic model with the different regions of etching presented on the normalized red component of a randomly selected grain in cast iron

By examining a single grain, reaching the first minimum requires significantly more time than it elapses between the following two or three extrema (t_d). It is the effect of the oxide layer protecting the surface at the start of the process. After that, for one or two half-cycles, a constant half-cycle time can be observed (t_{hc}). Later, however, the elapsed time will begin to increase again, indicating that diffusion through the growing layer is also a factor to be considered (t_{lag}). Thus, the etching process can be divided into three partially overlapping but well-detectable domains, as Figure 4 shows. In the functional model, the etching rate in the intermediate domain is constant and can be characterized by the steady-state etching rate (v_c) and the half-cycle time (t_{hc}). Half-cycle time can be determined by measuring the elapsed time between the first interference minimum and maximum.

By comparing the intensity curves of different grains to one another, the layer thickness for each grain should be the same at given extrema regardless of their orientation. The time required to reach their extrema, however, will differ, as more corrosion-resistant orientations will reach these extrema later. Consequently, the half-cycle time could be suitable to differentiate grains based on their etching rate without knowing the exact layer development rate after half-cycle times are assigned to the orientations determined by EBSD. By analyzing Figure 5, the half-cycle times show a strong correlation with $\langle 100 \rangle$, meaning that the etching rate is highest over grains with $\{100\}$ orientation.

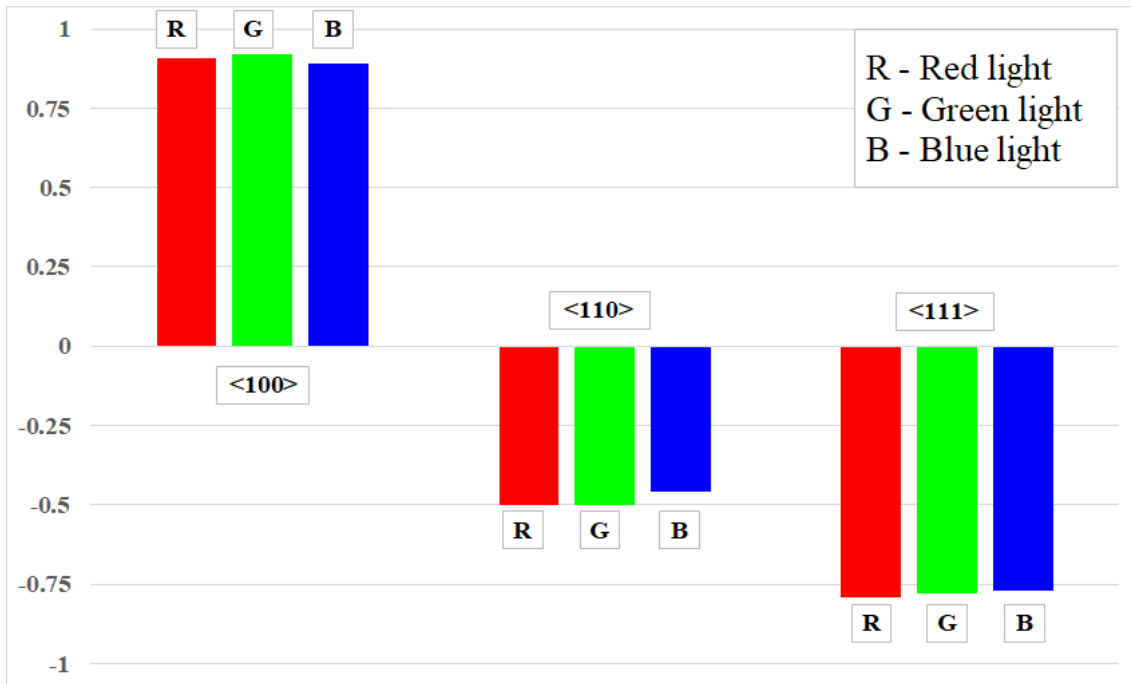


Figure 5. Correlation between the half-cycle time (t_{hc}) and the three main crystallographic orientations for the RGB components.

After determining the half-cycle times, atomic force microscopic (AFM) images were made to determine the thickness of the developed layer over the individual grains. By doing so, the orientation-dependent steady-state etching rates and the refractive indices for the investigated wavelengths were also determined.

To prove that the presented model is suitable for determining crystallographic orientation purely based on OM image processing, a new etching was performed over a randomly selected area. From this area, the half-cycle time for a group of new grains was determined. By knowing the function of the orientation-dependent etching rate from the previous experiment, each grain was assigned to an orientation.

Finally, validation was performed with EBSD by comparing the results of these two measurements. With the functional kinetic model using exclusively optical image processing, the orientation could be determined with an error for $\{100\}$ in the $\pm 5^\circ$ range with an average error of 2.9° compared to what was obtained with EBSD.

4.3. Chemical composition and homogeneity of the developed layer (P4, P6)

Although the functional model presented in the previous chapter is a relatively accurate method to determine crystallographic orientation, certain hypotheses and methods must be reevaluated to ensure the resulting error is not derived from them. Such as, the model assumed that the chemical composition, and thus, the refractive index are homogeneous for the whole developed layer. As the refractive index strongly influences the observed color, any derivation would result in a significant variance and reduce the accuracy of orientation estimation. Hence, the purpose of the following experiment was to investigate the homogeneity and chemical composition of the developed layer. For that purpose, X-ray photoelectron spectroscopy (XPS) and spectroscopic ellipsometry (SE) were used without microfluidic cells.

Spectroscopic ellipsometry is the main optical method used to characterize developed thin films (Fujiwara, 2003), (Aspnes, 2014), (Fujiwara & Collins, 2018). During the measurement, the ellipsometer illuminates the surface with a light of known polarization while measuring the changes in polarization due to reflection (Vedam, 1998). SE is substantially more sensitive than traditional reflectometry since it can measure the phase difference between the two polarization directions. Although SE is suitable for directly calculating the refractive index and the layer thickness from the fitted model, it has a limited resolution as the diameter of the spot is approx. 0.3 mm. To resolve this issue, among the possible mixing of the different phases and making direct thickness and refractive index measurements for individual grains available, the sample material was replaced with coarse-grained DC01 low-carbon steel.

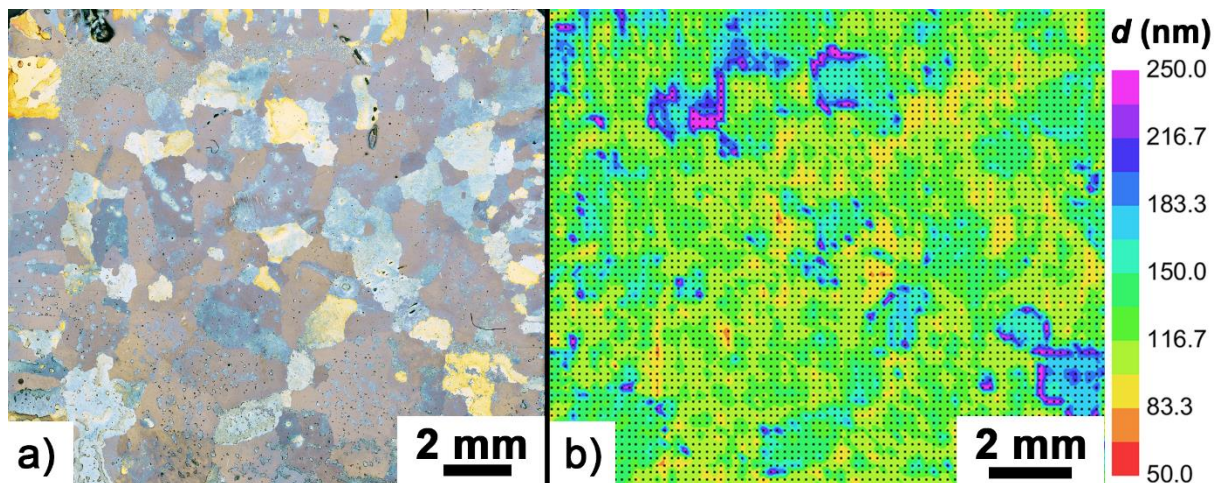


Figure 6. OM image of the color-etched ferritic steel specimen (a) and the layer thickness map (d) determined by SE (b)

To characterize the depth-dependent nature of the refractive index, two different approaches were applied. For the first method, the A parameter in the applied polynomial Cauchy dispersion formula was considered as constant for the whole layer. For the second approach, though, it was described with a monotonously decreasing exponential function along the thickness. Considering the nature of Cauchy dispersion, the parameter A is a good approximation of the refractive index. Thus, in the first case, the

refractive index is assumed constant, while in the second case, the refractive index continuously decreases as it moves away from the substrate's surface. Figure 6 presents the OM images right after stabilizing the layer and the layer thickness map of SE by using the first fitting method. As can be seen, the average grain size was large enough so that most of the grains were properly distinguishable.

Although the separability of grains in the layer thickness map was expected, based on the original hypothesis, the refractive index map and the means square error map of fitting should have been constant along the surface. Since the individual grains could be identified on those maps as well, they contradict the initial model, meaning that the parameter A should change along the thickness. This statement is also supported by the second fitting, where the refractive index decreased along the thickness because this way, the mean square error of fitting became negligibly small.

To further analyze data, the orientations of the individual grains were also determined with EBSD. This measurement, combined with XPS, not only supported the previous statement that the layer development rate is highest in the $\langle 100 \rangle$ direction and strongly correlates with the enclosed angle with it but also showed that the exponential decaying nature of the refractive index is also orientation dependent. Hence, the nature of exponential change also depends on the crystallographic orientation of the grain underneath it.

4.4. *Over-etching (P3, P7)*

Ferrite in low-carbon steel was etched significantly faster than in cast iron, thus, the thickness of the developed layer also increased much faster. The process was prolonged so far that most of the grains became over-etched. From the aspect of the investigation, reaching this state is avoidable, as the influence of diffusion is unknown, and the distinguishability of the surface starts to deteriorate.

Although over-etching is a widely used expression in various fields, it is nowhere defined, what is called "over-etched" in terms of color etching, and what is the limit after that a surface will reach this state (Hashimoto et al., 2002), (Qian & Sigmund, 2013), (Gasvoda et al., 2020). Thus, my next aim was to connect the concept of over-etching to a measurable physical phenomenon for color etching processes.

By knowing that the intensity of different light components could depend on various extrinsic factors, the direct comparison and evaluation of intensity curves may not show a fully representative image of the surface area. To eliminate these differences, the normalized brightness (luminance) was calculated from the individual RGB components. By using luminance, different wavelength components are used at the same time, thus, a more general picture can be drawn about the surface.

From the comparison of optical images and intensity curves, it can be stated that the ferrite grains in low-carbon steel will be over-etched after reaching their fourth local, or the third real maxima, considering that the beginning of the process should not be

treated as an extremum. For the investigated ferrite grains, Figure 7 presents the difference in luminance between the over-etched grain 1 and grain 3 that did not reach this state yet.

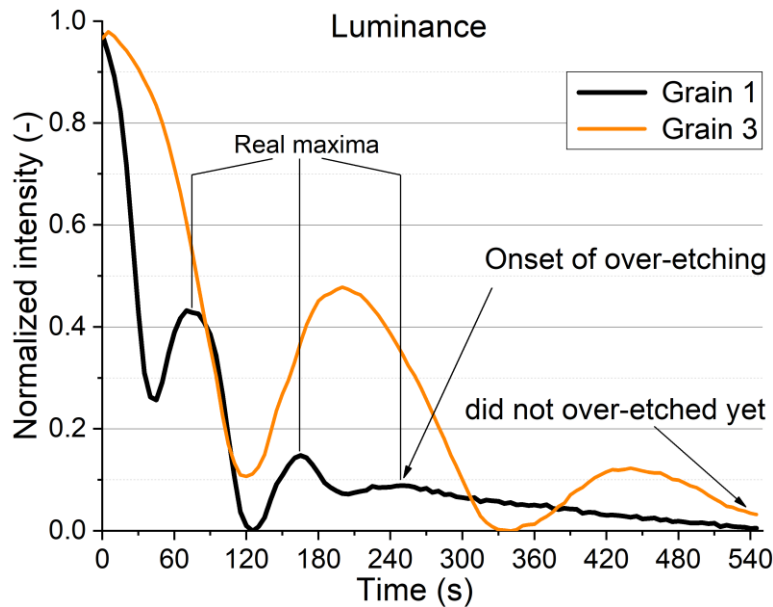


Figure 7. Luminance curves of grains 1 and 3 with important characteristic times on it

4.5. *In situ observation of color etching via spectroscopic ellipsometer*

After the investigation of the refractive index and the chemical composition, the next step is to directly measure the layer development during etching. By doing so, the second microfluidic cell designed for in-situ spectroscopic ellipsometry was used. The fitting model used for the in-situ characterization consisted of a metal substrate, a surface layer, and the etchant as the ambient from which the light accesses the surface. From this fitted model, layer thickness was determined, as shown in Figure 8.

The rapid changes of layer properties in the first 120 s involve a layer buildup to a thickness of almost 170 nm. After 120 s, a slight but continuous decrease starts. This indicates that the flow rate was increased to flush out the etchant, and the layer's not yet stabilized parts started a continuous detachment. This decrease can be utilized to determine the end of the etching process, marked with a purple line.

Due to its more complex geometry, the microfluidic cell for SE must be filled with distilled water prior to etching to ensure proper sealing and the removal of any air bubbles left in the light path. The hydrated initial state of the surface, however, results in a faster oxide breakthrough, reducing the necessary time to surpass the oxide-limited domain. That is why the growth is nearly constant during the etching process. Moreover, this continuous increase in layer thickness proves the existence of a steady-state etching rate in the early phases of the process.

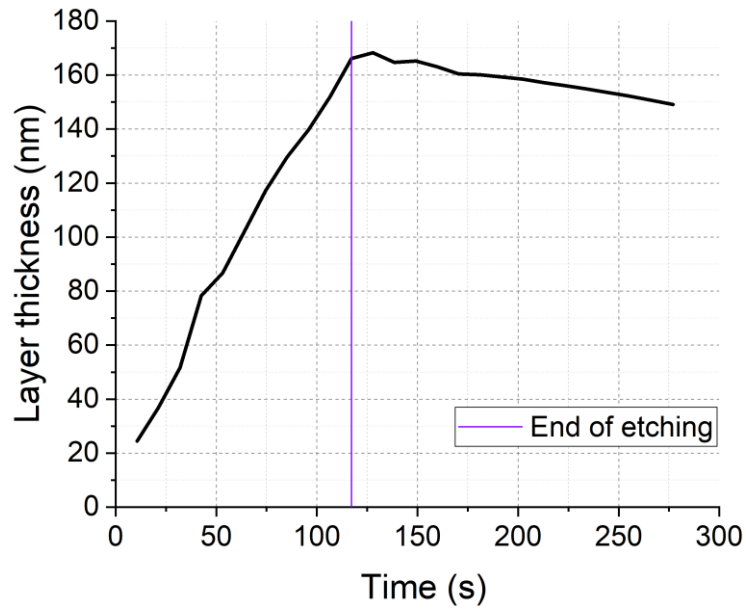


Figure 8. Layer thickness change during in-situ SE observation

4.6. Color etching of copper (P8)

In the previous chapters, only materials with ferritic phases were investigated. Although the color etching with Beraha-I has been thoroughly detailed, the observations should be extended to other lattice structures as well. For that purpose, Cu99.9 was chosen as it can also be etched by Beraha-I, but it has a face-centered cubic lattice compared to the ferrite's base-centered cubic one.

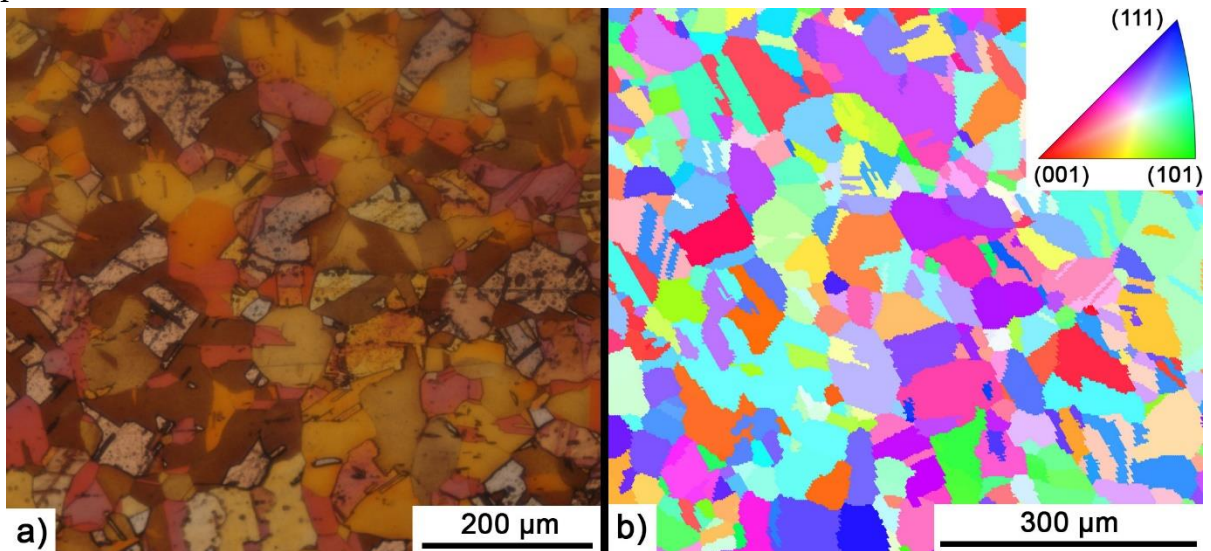


Figure 9. Optical microscope image (a) and EBSD map (b) of the investigated area in copper

The investigation of color etching in the microfluidic cell for OM showed that copper reacts similarly to ferrite, but it has significantly better corrosion resistance. Over the individual grains, a longer but dominantly cyclic color change occurs. Although this periodic change is detectable on multiple grains, some may behave differently. Certain

grains seem to develop a color early in the process, which they keep for the rest of the experiment. Based on this behavior, grains could be divided into three different groups. First, there are grains over which the cyclic color change occurs, as expected from previous experiments. The second and third groups both include grains with a single developed color, which doesn't undergo any significant change later. For these grains, the resulting constant color is either white or dark brown.

To investigate the correlation between color and orientation, an EBSD mapping was performed over the same area, as seen in Figure 9. By comparing the color information of the grains after etching with their crystallographic information from EBSD reveals some intriguing relationships. The orientations of grains that remained white are typically close to $\{100\}$, while dark brown grains are typically the farthest from $\{100\}$ and are relatively close to $\{122\}$. Other "regular" grains have a rather general orientation with a moderate enclosed angle with these directions.

Consequently, even if every grain produces the same cyclic characteristics regardless of their orientation, the difference is the result of a significant deviation in the absorption properties. Grains close to $\{100\}$ have an extraordinarily long half-cycle time, meaning that the decrease in absorption is almost completely neglectable. That is why the bright white color of these grains appeared to be unchanged. Grains close to $\{122\}$, on the other hand, had a very dominant absorption that resulted in the decay in the amplitude. This smoothed the differences in detectable color and ultimately caused a faster darkening due to the significant intensity loss.

This characteristic, however, can be utilized as a fast approximation method to determine the proportion of specific orientations over the surface. The two distinguished colors, namely white and dark brown, can be associated with the most densely and sparsely packed planes, and through these, the proportion of grains close to $\{100\}$ and $\{122\}$ as well.

5. NEW SCIENTIFIC RESULTS

Based on the color etching of different materials with Beraha-I etchant, I formulated the following scientific statements:

1. By using the functional kinetic model I developed combined with my microfluidic cell, it is possible to in-situ monitor the layer development during color etching process. Based on the tests carried out in this way, the layer development process can be divided into three stages:

1. Oxide layer limited etching
2. Steady-state etching
3. Diffusion-limited etching

With the separation of these stages, the investigation of the connection between color change and crystallographic orientation becomes possible (P1, P2, P5).

2. The interference and absorption of the developed layer heavily depend on the orientation, hence, the characteristic parameters of the intensity curve for a given light component (like half-cycle time or brightness change rate) can be assigned to certain orientations (P1, P4, P7, P8, P9).

3. For ferrite with a base-centered cubic lattice, the fastest etching rate occurs over grains with {100} orientation. For copper with a face-centered cubic lattice, however, the same orientation results in one of the slowest etching rates (P1, P3, P6, P9).

4. With the utilization of the functional kinetic model, the crystallographic orientation of ferrite in a cast iron sample can be determined with a $\pm 3^\circ$ average absolute error compared to EBSD only by evaluating the optical microscopic images of the color etching process (P1).

5. I proved that due to the orientation-dependent nature of color etching, the dissolution rate, and thus, the chemical composition of the formed layer will not only differ over the individual grains, but it will also gradually change along the thickness of a given grain. Considering that both the refractive index and the absorption coefficient strongly depend on the chemical composition, they will also change in the lateral direction (P4, P5, P7, P9).

6. Since earlier it was non-existent, I assigned the concept of over-etching to a measurable physical phenomenon for color etching processes. By using this definition, I found that the over-etching for ferrite in low-carbon steel occurs when the light intensity curve reaches its third real maximum (P3, P8).

6. PUBLICATIONS

- (P1) Bonyár, A., Renkó, J., Kovács, D., & Szabó, P. J. (2019). Understanding the mechanism of Beraha-I type color etching: Determination of the orientation dependent etch rate, layer refractive index and a method for quantifying the angle between surface normal and the $\langle 100 \rangle$, $\langle 111 \rangle$ directions for individual grains. *Materials Characterization*, 156. <https://doi.org/10.1016/j.matchar.2019.109844>
- (P2) Renkó, J. B., Bonyár, A., & Szabó, P. J. (2020). Development of Microfluidic Cell for Liquid Phase Layer Deposition Tracking. *Acta Materialia Transylvanica*, 3(2), 94–97. <https://doi.org/10.33924/AMT-2020-02-08>
- (P3) Renkó, J. B., Bonyár, A., & Szabó, P. J. (2020). Effect of Beraha-I type color etchant on the ferrite phase in different type Fe-C alloys. *IOP Conference Series: Materials Science and Engineering*, 903(1), 012054. <https://doi.org/10.1088/1757-899X/903/1/012054>
- (P4) Renkó, J. B., Romanenko, A., Szabó, P. J., Petrik, P., & Bonyár, A. (2021). Színesen mart ferrites acél vizsgálata spektroszkópiai ellipszometriával. *Bányászati És Kohászati Lapok - Kohászat*, 154(3–4), 32–36. www.ombkenet.hu/bkl/kohaszat.html
- (P5) Bíró, T., & Renkó, J. B. (2021). Design and Manufacture of a Microfluidic Cell To Be Used With a Spectroscopic Ellipsometer. *Acta Materialia Transylvanica*, 4(1), 28–31. <https://doi.org/10.33924/AMT-2021-01-05>
- (P6) Renkó, J. B., Romanenko, A., Szabó, P. J., Petrik, P., & Bonyár, A. (2021). Analysis of the microstructure of color etched low carbon steel with spectroscopic ellipsometry. *Symposium on Materials Science*, 1, 20–24.
- (P7) Renkó, J. B., Romanenko, A., Szabó, P. J., Sulyok, A., Petrik, P., & Bonyár, A. (2022). Analysis of structural and chemical inhomogeneity of thin films developed on ferrite grains by color etching with Beraha-I type etchant with spectroscopic ellipsometry and XPS. *Journal of Materials Research and Technology*, 18, 2822–2830. <https://doi.org/10.1016/J.JMRT.2022.03.159>
- (P8) Renkó, J. B., & Szabó, P. J. (2022). Investigation of the Effect of Over-Etching During Color Etching. *Acta Materialia Transylvanica*, 5(1), 29–34. <https://doi.org/10.33924/AMT-2022-01-07>
- (P9) Renkó, J. B., Szabó, P. J., & Bonyár, A. (2023). Correlation between the developed layer's color and crystallographic orientation of pure copper during long-term color etching with Beraha-I. *Journal of Materials Research and Technology*, 23, 4346–4354. <https://doi.org/10.1016/J.JMRT.2023.02.082>

7. REFERENCES

- Aspnes, D. E. (2014). Spectroscopic ellipsometry — Past, present, and future. *Thin Solid Films*, 571(P3), 334–344. <https://doi.org/10.1016/J.TSF.2014.03.056>
- Bonyár, A., Sántha, H., Ring, B., Varga, M., Kovács, J. G., & Harsányi, G. (2010). 3D Rapid Prototyping Technology (RPT) as a powerful tool in microfluidic development. *Procedia Engineering*, 5, 291–294. <https://doi.org/10.1016/J.PROENG.2010.09.105>
- Bonyár, A., & Szabó, P. J. (2012). Correlation between the grain orientation dependence of color etching and chemical etching. *Microscopy and Microanalysis*, 18(6), 1389–1392. <https://doi.org/10.1017/S1431927612013554>
- Britz, D., Hegetschweiler, A., Roberts, M., & Mucklich, F. (2016). Reproducible Surface Contrasting and Orientation Correlation of Low-Carbon Steels by Time-Resolved Beraha Color Etching. *Materials Performance and Characterization*, 5(5), 553–563. <https://doi.org/10.1520/MPC20160067>
- Fleißner-Rieger, C., Pogrietz, T., Obersteiner, D., Pfeifer, T., Clemens, H., Mayer, S., Fleißner-Rieger, C., Pogrietz, T., Obersteiner, D., Clemens, H., & Pfeifer, T. (2021). An Additively Manufactured Titanium Alloy in the Focus of Metallography. *Practical Metallography*, 58(1), 4–31. <https://doi.org/10.1515/PM-2020-0001>
- Fujiwara, H. (2003). *Spectroscopic Ellipsometry: Principles and Applications*. Maruzen Co. Ltd. https://books.google.hu/books?hl=hu&lr=&id=tTMn0NKcpjsC&oi=fnd&pg=PR7&dq=spectroscopic+ellipsometry&ots=NsU_rqOWuP&sig=R2Kmtj7KNzGFexA4y5ohm1wFEnk&redir_esc=y#v=onepage&q=spectroscopic%20ellipsometry&f=false
- Fujiwara, H., & Collins, R. W. (2018). *Spectroscopic Ellipsometry for Photovoltaics* (H. Fujiwara & R. W. Collins, Eds.; 1st ed., Vol. 1). Springer International Publishing. <https://doi.org/10.1007/978-3-319-75377-5>
- Gasvoda, R. J., Zhang, Z., Wang, S., Hudson, E. A., & Agarwal, S. (2020). Etch selectivity during plasma-assisted etching of SiO₂ and SiN_x: Transitioning from reactive ion etching to atomic layer etching. *Journal of Vacuum Science & Technology A: Vacuum, Surfaces, and Films*, 38(5), 050803. <https://doi.org/10.1116/6.0000395>
- Hamelin, A. (1984). Underpotential deposition of lead on single crystal faces of gold: Part I. The influence of crystallographic orientation of the substrate. *Journal of Electroanalytical Chemistry and Interfacial Electrochemistry*, 165(1–2), 167–180. [https://doi.org/10.1016/S0022-0728\(84\)80095-9](https://doi.org/10.1016/S0022-0728(84)80095-9)
- Hashimoto, M., Ohno, H., Kaga, M., Sano, H., Tay, F. R., Oguchi, H., Araki, Y., & Kubota, M. (2002). Over-etching effects on micro-tensile bond strength and failure patterns for two dentin bonding systems. *Journal of Dentistry*, 30(2–3), 99–105. [https://doi.org/10.1016/S0300-5712\(02\)00004-0](https://doi.org/10.1016/S0300-5712(02)00004-0)
- Hölscher, M., Raabe, D., & Lücke, K. (1991). Rolling and recrystallization textures of body centered cubic steels. *Steel Research*, 62(12), 567–575. <https://www.dierk-raabe.com/app/download/5807275577/Overview+textures+steels.pdf>
- Jovičević-Klug, P., Lipovšek, N., Jovičević-Klug, M., & Podgornik, B. (2021). Optimized preparation of deep cryogenic treated steel and Al-alloy samples for optimal microstructure imaging results. *Materials Today Communications*, 27, 102211. <https://doi.org/10.1016/J.MTCOMM.2021.102211>
- Kardos, I., & Gácsi, Z. (2013). Investigation of Microstructure of Cast Iron by Color Etching. *Materials Science Forum*, 752, 167–174. <https://doi.org/10.4028/WWW.SCIENTIFIC.NET/MSF.752.167>
- Kardos, I., Gácsi, Z., & Szabó, P. J. (2007). Color Etching for Characterization the Grain Orientation in Spheroidal Graphite Cast Iron. *Materials Science Forum*, 537–538, 389–396. <https://doi.org/10.4028/WWW.SCIENTIFIC.NET/MSF.537-538.389>
- Mandal, M., Aashranth, B., Samantaray, D., & Vasudevan, M. (2022). Improvements in the Metallography of Ferritic–Martensitic Steels Through a Color Etching Procedure. *Metallography, Microstructure, and Analysis*, 1–13. <https://doi.org/10.1007/S13632-022-00916-0/FIGURES/11>

- Medina-Mendoza, J. A., Mayen-Chaires, J., Mercado-Lemus, V. H., & Pérez-Bustamante, R. (2022). Color Etching of a MIG Welded Steel Joint. *Microscopy and Microanalysis*, 28(S1), 2786–2787. <https://doi.org/10.1017/S1431927622010510>
- Monteiro, W. A., Silva, E. M. R., Silva, L. V., De Rossi, W., & Buso, S. J. (2010). Microstructural and Mechanical Characterization of Gray Cast Iron and AlSi Alloy after Laser Beam Hardening. *Materials Science Forum*, 638–642, 769–774. <https://doi.org/10.4028/WWW.SCIENTIFIC.NET/MSF.638-642.769>
- Newesely, H., & Rabe, H. (1985). Metallographic texture analysis of dental materials by polarizing microscopy in the incidental light. *Journal of Biomedical Materials Research*, 19(4), 369–380. <https://doi.org/10.1002/JBM.820190403>
- Panagopoulos, C. N., Georgiou, E. P., & Gavras, A. G. (2009). Corrosion and wear of 6082 aluminum alloy. *Tribology International*, 42(6), 886–889. <https://doi.org/10.1016/J.TRIBOINT.2008.12.002>
- Panda, S., Sahoo, S. K., Dash, A., Bagwan, M., Kumar, G., Mishra, S. C., & Suwas, S. (2014). Orientation dependent mechanical properties of commercially pure (cp) titanium. *Materials Characterization*, 98, 93–101. <https://doi.org/10.1016/J.MATCHAR.2014.10.011>
- Qian, X., & Sigmund, O. (2013). Topological design of electromechanical actuators with robustness toward over- and under-etching. *Computer Methods in Applied Mechanics and Engineering*, 253, 237–251. <https://doi.org/10.1016/J.CMA.2012.08.020>
- Rawdon, H. S., & Lorentz, M. G. (1920). *Scientific Papers of the Bureau of Standards - No. 399. Metallographic etching reagents: I, for copper* (Vol. 16). National Bureau of Standards. <https://archive.org/details/metallographicet16641rawd/page/n3/mode/2up>
- Tran, R., Li, X. G., Montoya, J. H., Winston, D., Persson, K. A., & Ong, S. P. (2019). Anisotropic work function of elemental crystals. *Surface Science*, 687, 48–55. <https://doi.org/10.1016/J.SUSC.2019.05.002>
- Vander Voort, G. F. (1984). *Metallography, Principles and Practice*. In *New York, McGraw-Hill Book Co.* New York McGraw-Hill Book Co. https://books.google.hu/books?hl=hu&lr=&id=GRQC8zYqtBIC&oi=fnd&pg=PR12&dq=etching+metallography&ots=_zl-U6AyIV&sig=LSbx5Ig_6qxsVrb0mNN8NFc1B28&redir_esc=y#v=onepage&q=etching%20metallography&f=false
- Vander Voort, G. F. (Ed.). (1985). *ASM Metals Handbook, Vol. 9 Metallography and microstructures* (Vol. 9). ASM International. <https://docs.google.com/file/d/0B3Mrzn2Z7-tSbURmRThQQnh6Skk/edit?resourcekey=0-bWLFd0aUKlQJBs7laEr31Q>
- Vander Voort, G. F. (1986). *Applied Metallography: Phase Identification by Selective Etching*. In G. F. Vander Voort (Ed.), *Applied Metallography* (1st ed.). Springer. https://doi.org/10.1007/978-1-4684-9084-8_1
- Vander Voort, G. F. (2004). Color metallography. In G. F. Vander Voort (Ed.), *ASM handbook* (Vol. 9, pp. 493–512). ASM International. <https://doi.org/10.1361/asmhba0003752>
- Vander Voort, G. F., & Manilova, E. P. (2023). *Metallographic Etching of Aluminum and Its Alloys*. <https://docplayer.net/38808493-Metallographic-etching-of-aluminum-and-its-alloys.html>
- Vedam, K. (1998). Spectroscopic ellipsometry: a historical overview. *Thin Solid Films*, 313–314, 1–9. [https://doi.org/10.1016/S0040-6090\(97\)00762-1](https://doi.org/10.1016/S0040-6090(97)00762-1)
- Yardley, V. A., Fahimi, S., & Payton, E. J. (2014). Classification of creep crack and cavitation sites in tempered martensite ferritic steel microstructures using MTEX toolbox for EBSD. *Materials Science and Technology*, 10(1), 547–553. <https://doi.org/10.1179/1743284714Y.0000000603>